Lyapunov Estimator for High-Speed Demodulation in Dynamic Mode Atomic Force Microscopy

Michael R. P. Ragazzon, Michael G. Ruppert, David M. Harcombe, Andrew J. Fleming, J. Tommy Gravdahl

***Abstract*—In dynamic mode atomic force microscopy (AFM), the imaging bandwidth is governed by the slowest component in the open-loop chain consisting of the vertical actuator, cantilever and demodulator. While the common demodulation method is to use a lock-in amplifier (LIA), its performance is ultimately bounded by the bandwidth of the post-mixing low-pass filters. This article proposes an amplitude and phase estimation method based on a strictly positive real Lyapunov design approach. The estimator is designed to be of low complexity while allowing for high bandwidth. Additionally, suitable gains for high performance are suggested such that no tuning is necessary. The Lyapunov estimator is experimentally implemented for amplitude demodulation and shown to surpass the LIA in terms of tracking bandwidth and noise performance. High-speed AFM images are presented to corroborate the results.**

***Index Terms*—Amplitude estimation, atomic force microscopy (AFM), Lyapunov methods, parameter estimation, nanopositioning, phase estimation, Kalman filters.**

I. Introduction

ATOMIC Force Microscopy (AFM) has become a key enabling technology for high-precision study of materials and biological processes over the last few decades [1]. The dynamic modes of AFM [2] are particularly well suited for studying soft biological materials due to the small friction and interaction forces involved [3], [4]. In dynamic mode AFM, a cantilever is forced to oscillate over the sample surface. As the cantilever approaches the surface, the amplitude and phase of the oscillation becomes a function of the sample topography. By demodulating the amplitude or phase and using them in a feedback loop with the vertical positioner, the cantilever is made to follow the surface as illustrated in Fig. 1. In order to obtain the sample topography, the cantilever is commonly scanned in a raster pattern along the lateral directions.

The imaging bandwidth is limited by the slowest component in the control loop consisting of the vertical actuator, cantilever, and demodulator [5]. The vertical actuator is commonly constructed from a piezoelectric element and the bandwidth is highly dependent on its mechanical design [6]. The cantilever bandwidth on the other hand is limited by its resonance frequency f_0 and quality (Q) factor by $f_0/(2Q)$ [5]. Thus, a cantilever with high resonance frequency and preferably low Q factor is typically chosen for high-speed AFM applications.

M.R.P. Ragazzon and J.T. Gravdahl are with the Department of Engineering Cybernetics, NTNU, Norwegian University of Science and Technology, Trondheim, Norway. Email: ragazzon@itk.ntnu.no, Tommy.Gravdahl@itk.ntnu.no.

M.G. Ruppert, D.M. Harcombe and A.J. Fleming are with the School of Electrical Engineering and Computer Science, University of Newcastle, Callaghan NSW 2308, Australia. Email: Michael.Ruppert@uon.edu.au, David.Harcombe@uon.edu.au, Andrew.Fleming@newcastle.edu.au.

Finally, a high bandwidth demodulator is necessary to complete the control loop which is the primary focus of this article. The most common demodulator in AFM applications is the lock-in amplifier, which is a type of synchronous demodulator where the carrier reference signal is known. In their simplest form, these amplifiers consist of a multiplier followed by a low-pass filter [7]. Although lock-in amplifiers can provide a high noise rejection, the performance is ultimately limited by the bandwidth of the post-mixing low-pass filters.

Several high-bandwidth amplitude demodulation techniques have been proposed for increasing the overall imaging bandwidth. The high-speed AFM results presented in [8] introduce the peak hold method which converges in half an oscillation cycle. However, this method is prone to noise and disturbances from unwanted harmonics. Recent developments include the low-latency coherent demodulator [9], the high-bandwidth lock-in amplifier [10], and Kalman filter [11], [12]. The latter has also been extended for multiharmonic imaging [13], [14]. The performance of several of these methods and others was numerically evaluated in [15], where the Lyapunov-based amplitude estimator was introduced in brief. This adaptive law based on a strictly positive real Lyapunov design approach [16] – or Lyapunov estimator – was shown to strike a good balance between performance and complexity.

Although the Kalman filter results were shown to be effective in terms of performance, the complexity of implementing a complete Kalman filter in a high-speed setting can be challenging. In fact, the computational complexity of the update law can ultimately become a limiting factor in terms of allowable bandwidth. Additionally, with simpler update laws the sampling speed can be increased which will reduce the overall noise floor of the system [17]. Thus, a simpler estimator was sought with similar performance characteristics,

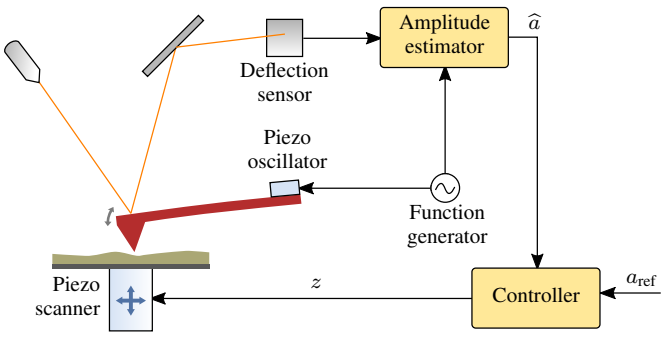

Fig. 1. Amplitude modulated operating mode in AFM.

which resulted in the Lyapunov estimator. This estimator can be seen as a simplification of the Kalman filter in terms of the update laws and computational complexity, without sacrificing significant performance.

In this article the Lyapunov estimator is described in detail, including convergence properties, implementation and tuning details, and experimental results.

The remainder of the article proceeds as follows. In Sec. II the amplitude estimation problem is formulated. Background material for the general Lyapunov estimator is provided in Sec. III, and stability properties and convergence rate are established. In Sec. IV the Lyapunov amplitude estimator is presented. Sec. V provides procedures for tuning the estimator. Experimental results are discussed in Sec. VI. Finally, conclusions are drawn in Sec. VII.

Notation: Time-domain signals are denoted lower-case, e.g. $y(t)$, while frequency-domain filters are denoted upper-case as in $W(s)$. The time-dependency of a signal is often not explicitly stated for convenience. Furthermore, filters and signals are sometimes mixed, e.g., the expression $z(t) = W(s)y(t)$ should be understood as $z(t) = \mathcal{L}^{-1}\left[W(s)\mathcal{L}(y(t))\right]$ where $\mathcal{L}$ is the Laplace transformation. Vector signals are denoted in bold such as $\mathbf{x}(t)$.

II. Problem Formulation

The problem can be formulated as estimating the amplitude $a(t)$ and phase $\phi(t)$ using only past and present measurements of the signal

$$y(t) = a(t)\sin(\omega_0 t + \phi(t)) + v(t), \tag{1}$$

where ω_0 is the known angular frequency and $v(t)$ represents a zero-mean noise process. Optionally, the signal is measured through a device or filtered through a transfer function $W(s)$ such that

$$z = W(s)y \tag{2}$$

where z is the input signal exposed to the estimator. This transfer function can either represent a part of the plant such as a measuring device, or alternatively be implemented as a signal processing filter as part of the estimator, such as for noise attenuation. The filter can be assumed unitary $W(s) = 1$ if not desired.

III. Estimator Background

In this section background material for the Lyapunov estimator is presented. The problem needs to be transformed into a model suitable for application of the general Lyapunov parameter estimator. Some insight into the stability properties of the estimator is provided. More specifically for the problem at hand, it is shown that the estimator guarantees convergence of the parameter estimates in exponential time due to the persistently exciting (PE) property of the signal vector. Additionally, a conservative limit on the convergence speed of the method is found for the given signal vector. This allows easy tuning of the gain γ later.

A. Linear Parametric Model

The sinusoidal signal (1) can be written in terms of its in-phase and quadrature component by applying trigonometric identities such that

$$\begin{aligned} y &= a\sin(\omega_0 t + \phi) && (3)\\ &= a\cos(\phi)\sin(\omega_0 t) + a\sin(\phi)\cos(\omega_0 t) && (4)\\ &= \mathbf{c}^T\mathbf{x}, && (5)\end{aligned}$$

where noise has been disregarded, $\mathbf{x} = [x_1, x_2]^T$, and

$$\mathbf{c} = \left[\sin(\omega_0 t),\, \cos(\omega_0 t)\right]^T. \tag{6}$$

The system is now in a linear-in-the-parameters form, which permits the direct application of estimation methods [16]. By comparing (4) and (5) the amplitude and phase can be found from

$$\begin{aligned} a &= \|\mathbf{x}\|_2, && (7)\\ \phi &= \operatorname{atan2}\left(x_2, x_1\right), && (8)\end{aligned}$$

where $\operatorname{atan2}(\cdot)$ is the four-quadrant tangent inverse function.

B. SPR Property of $W(s)$

A necessary condition for the stability of the estimator requires the transfer function $W(s)$ to be strictly positive real (SPR). Positive realness of a transfer function is related to the passivity of a system, see e.g. [16], [18], [19]. The following definitions are restated here for convenience:

Definition 1: A rational proper transfer function $W(s)$ is *positive real* (PR) if

- $W(s)$ is real for real s.
- $\operatorname{Re}\left[G(s)\right] \geq 0$ for all $\operatorname{Re}[s] > 0$.

Definition 2: Assume that $W(s)$ is not identically zero for all s. Then $W(s)$ is called *strictly positive real* if $W(s-\varepsilon)$ is PR for some $\varepsilon > 0$.

Remark 1: If the desired $W(s)$ is not SPR, it can be modified by introducing a transfer function $L(s)$ such that the new filter $W^*(s) = W(s)L(s)$ is SPR and replaces $W(s)$. If no proper $L(s)$ can be found, the signals $y(t)$ and $\mathbf{c}(t)$ themselves can be filtered to allow the estimator to be realizable. This is further discussed in [16], [20].

C. General Lyapunov Estimator

The estimator is based on a Lyapunov approach from [16] for a wide class of systems of the linear parametric form such as in (5) with unknown parameters $\mathbf{x}$. The Lyapunov estimator allows the estimated parameters $\widehat{\mathbf{x}}$ to be found from the input signal z and the known signal vector $\mathbf{c}$. The estimator can be written as

$$\begin{aligned} \dot{\widehat{\mathbf{x}}} &= \gamma\mathbf{c}\left(z - \widehat{z}\right), && (9)\\ \widehat{z} &= W(s)\mathbf{c}^T\widehat{\mathbf{x}} && (10)\end{aligned}$$

where γ is a constant gain parameter and $\widehat{z}$ is the estimated input signal. In general, an additional normalization term is applied to (9) in case the signal vector $\mathbf{c}$ is unbounded, this is not necessary in the case of (6). Additional details are found in [16].

D. Stability

The update law (9) applies for a wide range of problems and guarantees boundedness of the error $\varepsilon = z - \widehat{z}$ and the estimate $\widehat{\mathbf{x}}$. The stability properties of the estimator can be shown using the Lyapunov-like function

$$V(\tilde{\mathbf{x}}, \mathbf{e}) = \frac{\mathbf{e}^T \mathbf{P}_c \mathbf{e}}{2} + \frac{\tilde{\mathbf{x}}^T \gamma^{-1} \tilde{\mathbf{x}}}{2} \tag{11}$$

where $\mathbf{P}_c = \mathbf{P}_c^T > 0$, $\tilde{\mathbf{x}} = \mathbf{x} - \widehat{\mathbf{x}}$, and $\mathbf{e}$ is the state vector of the state-space representation of the error signal which can be found to be $\varepsilon = W(s)\mathbf{c}^T\tilde{\mathbf{x}}$. The SPR property of $W(s)$ is exploited in the derivation of the update law (9) canceling the indefinite terms of $\dot{V}$ such that it becomes negative semidefinite. This immediately guarantees boundedness – that is $\mathcal{L}_\infty$-stability of $\varepsilon, \widehat{\mathbf{x}}$, and $\mathcal{L}_2$-stability of $\varepsilon, \dot{\widehat{\mathbf{x}}}$ [16, Thm. 4.3.1]. However, this does not yet guarantee convergence of the parameters which is essential for the amplitude estimation problem. An additional persistency of excitation property of the signal $\mathbf{c}$ is necessary.

E. Persistency of Excitation

Although the parameter estimates are guaranteed to be bounded, an additional persistency of excitation (PE) [16] property of the signal vector $\mathbf{c}$ is required for convergence of the parameters. In the following it is shown that $\mathbf{c}$ given in (6) is PE.

The signal is PE if there exists constants $T, \alpha_0, \alpha_1 > 0$ such that

$$\alpha_1 \mathbf{I} \geq \mathbf{S} \triangleq \frac{1}{T}\int_t^{t+T} \mathbf{c}(\tau)\mathbf{c}^T(\tau)d\tau \geq \alpha_0 \mathbf{I} \quad \forall\, t \geq 0. \tag{12}$$

Evaluating $\mathbf{S}$ with $\mathbf{c}$ from (6) gives

$$\mathbf{S} = \frac{1}{4T\omega_0}\begin{bmatrix} 2\omega_0 T - \sin\left(2\omega_0\left(T+t\right)\right) + \sin\left(2\omega_0 t\right) & \\ -\cos\left(2\omega_0\left(T+t\right)\right) + \cos\left(2\omega_0 t\right) & \\ -\cos\left(2\omega_0\left(T+t\right)\right) + \cos\left(2\omega_0 t\right) & \\ 2\omega_0 T + \sin\left(2\omega_0\left(T+t\right)\right) - \sin\left(2\omega_0 t\right) & \end{bmatrix} \tag{13}$$

and choosing

$$T = \tfrac{1}{2} f_0^{-1} = \pi \omega_0^{-1} \tag{14}$$

results in

$$\mathbf{S} = \begin{bmatrix} \frac{1}{2} & 0 \\ 0 & \frac{1}{2} \end{bmatrix} = \tfrac{1}{2}\mathbf{I} \quad \forall\, t \geq 0 \tag{15}$$

with a level of excitation $\alpha_0 = \frac{1}{2}$. Thus, $\mathbf{c}$ from (6) is PE which guarantees exponential convergence of $\widehat{\mathbf{x}} \to \mathbf{x}$ [16, Cor. 4.3.1].

F. Convergence Rate and Gain γ

Given the PE property of the signal vector $\mathbf{c}$, the parameter estimates are guaranteed to converge in exponential time. In fact, the rate of convergence can be found in terms of the gain γ. An expression for γ can then be found which optimizes the rate of convergence as shown in the following.

For ease of analysis, assume here that $W(s) = 1$ which makes the update law (9)-(10) equivalent to the update law of the gradient method [16], which can be considered a special case of the Lyapunov estimator. Then, the convergence of the parameter estimate error $\tilde{\mathbf{x}}(t)$ is determined by [16]

$$\tilde{\mathbf{x}}^T\tilde{\mathbf{x}} \leq k^n \tilde{\mathbf{x}}_0^T \tilde{\mathbf{x}}_0, \quad \forall\, t \geq nT,\ n = 0, 1, \ldots \tag{16}$$

for $\tilde{\mathbf{x}}_0 = \tilde{\mathbf{x}}(0)$ and $0 < k < 1$ given by

$$k = 1 - \frac{2\alpha_0 T\gamma}{2 + \beta^4 T^2 \gamma^2} \tag{17}$$

where $\beta = \sup_t |\mathbf{c}(t)| = 1$ for $\mathbf{c}$ in (6). Thus, the convergence rate is given by k such that a smaller value gives faster convergence.

The gain γ minimizing k in (17) can now be found. Inserting for T from (14) and α_0 found from (15) results in

$$\arg\min_\gamma k = 2\sqrt{2} f_0. \tag{18}$$

This value of γ serves as a suitable initial choice. However, since the convergence rate in (16) represents a conservative limit due to the inherent conservative nature of Lyapunov analysis, a faster solution may be found through simulations.

IV. Lyapunov Amplitude and Phase Estimator

A. Update Law

In summary, the update law for the amplitude estimator is given by the Lyapunov estimator (9)-(10) applied to the system (5)-(6). Finally, the estimated amplitude $\widehat{a}$ and phase $\widehat{\phi}$ can be found by applying the parameter estimate $\widehat{\mathbf{x}}$ into (7)-(8).

Since $\widehat{\mathbf{x}}$ converges in exponential time, it is clear that $(\widehat{a}, \widehat{\phi}) \to (a, \phi)$ in exponential time considering (7)-(8). Some implementations of atan2 may not be defined for $\widehat{\mathbf{x}} = 0$. However, because of the exponential convergence properties the estimator can not stay identically in $\widehat{\mathbf{x}} = 0$ unless $y \equiv 0$, thus the issue is resolved in finite time for a well-posed problem. A block-diagram of the update law is shown in Fig. 2.

B. Relationship to the Kalman filter

Under certain conditions the Kalman filter for amplitude estimation [12] is equivalent to the Lyapunov estimator, as will be demonstrated in the following. First, it is shown that the two methods are equivalent when the covariance matrix of the Kalman filter, $\mathbf{P}$, is constant. Then, certain conditions under which the covariance matrix approaches constant is given, thus showing equivalency.

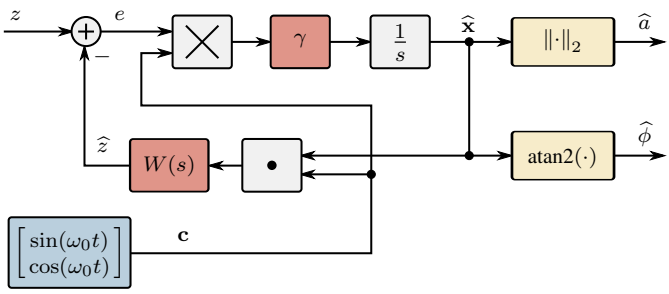

Fig. 2. Block diagram of the estimator. The blocks '$\cdot$' and '$\times$' represent vector dot product and matrix multiplication respectively.

With a system matrix $\mathbf{A} = 0$ and no input signal, $\mathbf{B} = 0$, the continuous-time Kalman filter can be written as

$$\dot{\hat{\mathbf{x}}} = \mathbf{P}\mathbf{c}\mathbf{R}^{-1}(z - \mathbf{c}^T\hat{\mathbf{x}}), \tag{19}$$

$$\dot{\mathbf{P}} = \mathbf{Q} - \mathbf{P}\mathbf{c}\mathbf{R}^{-1}\mathbf{c}^T\mathbf{P} \tag{20}$$

where the process covariance $\mathbf{Q}$ and measurement covariance $\mathbf{R}$ are assumed to be on the form $\mathbf{Q} = q\mathbf{I}, \mathbf{R} = r\mathbf{I}$ for some positive constants q, r.

Note that for $\dot{\mathbf{P}} = 0, \mathbf{P} = p\mathbf{I}$, the Kalman filter (19) is equivalent to the Lyapunov estimator (9)–(10) with $W(s) = 1$ and $\gamma = pr^{-1}$. Thus, in cases where $\mathbf{P}$ is constant, the Kalman filter can be reduced to the Lyapunov estimator with mathematical equivalency. In the following, solutions to the Kalman equations with constant $\mathbf{P}$ are found and investigated.

Consider a particular solution to (20) of the form

$$\mathbf{P} = \begin{bmatrix} a\sin(2\omega_0 t + \phi) + b & a\cos(2\omega_0 t + \phi) \\ a\cos(2\omega_0 t + \phi) & -a\sin(2\omega_0 t + \phi) + b \end{bmatrix} \tag{21}$$

for some constants a, b, ϕ. The real, positive solution to these constants in terms of ω_0, r, q are given by

$$a = \frac{q}{2\omega_0}, \tag{22}$$

$$b = \frac{\sqrt{q}\sqrt{q + 4\omega_0\sqrt{r^2\omega_0^2 + qr} + 4r\omega_0^2}}{2\omega_0}, \tag{23}$$

$$\phi = 2\mathrm{atan}\left(\sqrt{\frac{q - 4\omega_0\sqrt{r^2\omega_0^2 + qr} + 4r\omega_0^2}{q - 8r\omega_0^2}}\right). \tag{24}$$

In some cases the covariance matrix $\mathbf{P}$ approaches a constant, consider

$$\lim_{\omega_0 \to \infty} a/b = 0. \tag{25}$$

Thus, with increasing oscillation frequency the amplitude a in the covariance matrix is dominated by the constant offset term b and can be approximated by $\mathbf{P} = b\mathbf{I}$. In this case the Kalman filter can be simplified to the Lyapunov estimator with $W(s) = 1$ and

$$\gamma = b/r. \tag{26}$$

In fact, this equation can be used to tune the Lyapunov estimator if the measurement and process noise covariances are known. Additionally,

$$\lim_{q \to 0} a/b = 0, \tag{27}$$

$$\lim_{r \to \infty} a/b = 0. \tag{28}$$

Thus, the Kalman filter behaves identically to the Lyapunov estimator in the cases where

- the oscillation frequency ω_0 is large
- the process noise covariance q is small
- the measurement noise covariance r is large

In these cases, by replacing the Kalman filter with the Lyapunov estimator, the estimator can be run at higher update speeds possibly allowing for a higher bandwidth and improved noise response, due to the simpler implementation of the latter.

V. Tuning and Simulations

A. Simulation Results

Simulations for both amplitude and phase demodulation are plotted in Fig. 3 for different values of γ, measurement noise, and low-pass filter $W(s)$, implemented at a sampling rate of $4\,\mathrm{MHz}$. In general, it can be seen that for higher values of γ the estimator converges faster but at some point it starts to overshoot. When noise is added in Fig. 3 (b) it can be seen that high values of γ are more prone to noise. However, by applying a low-pass filter for $W(s)$ on the measured signal $y(t)$, some of the high-frequency noise is attenuated even at high γ values. The performance of the phase demodulation closely follows that of the amplitude demodulation, which is expected as they are both immediate calculations from the same estimated in-phase and quadrature components ($\hat{\mathbf{x}}$). Thus, the dynamics of the two demodulation modes should be equivalent.

B. Choosing the Transfer Function $W(s)$

The strictly positive real transfer function $W(s)$ can either represent any device or system between the sinusoidal signal $y(t)$ as in (1) and the estimator, and/or be designed as a post-measurement filter for reducing high-frequency noise. Otherwise, it can be assumed that the measurement $z(t)$ closely resembles that of the signal $y(t)$ by setting $W(s) = 1$. If instead, a low-pass filter is used, the bandwidth should be set high enough such that the oscillation frequency of the sinusoid in $y(t)$ is not attenuated.

C. Choosing the Gain γ

With an initial estimate of γ given by (18), further adjustments can be made by investigating the transient effect in the step response simulations in Fig. 3. It can be seen that for the highest value of the gain, $\gamma = 24f_0$ the transient overshoots considerably, while at $\gamma = 9f_0$ (red) it is seemingly close to critically damped. For lower values of γ the convergence rate is noticeably slower. The simulations thus suggest a value of

$$\gamma = 9f_0 \tag{29}$$

which, as expected, is slightly higher than the initial conservative estimate from (18).

Note that this evaluation is based on finding a gain primarily for achieving the highest possible estimation bandwidth. In some cases this may result in a noisy amplitude estimate. As demonstrated in the simulation results, by reducing the value of γ the estimator essentially acts as a low-pass filter on the noise, improving the noise rejection.

D. DC-Offset

In dynamic mode AFM there is typically a DC-offset in the measured cantilever deflection. A constant offset in the input signal $\mathbf{z}$ can affect the output response of the estimator, as demonstrated in Fig. 4. In general, this problem is most prominent at higher demodulator bandwidths. One solution for handling this is to use AC-coupling on the experimental measurement equipment, or equivalently adding a high-pass

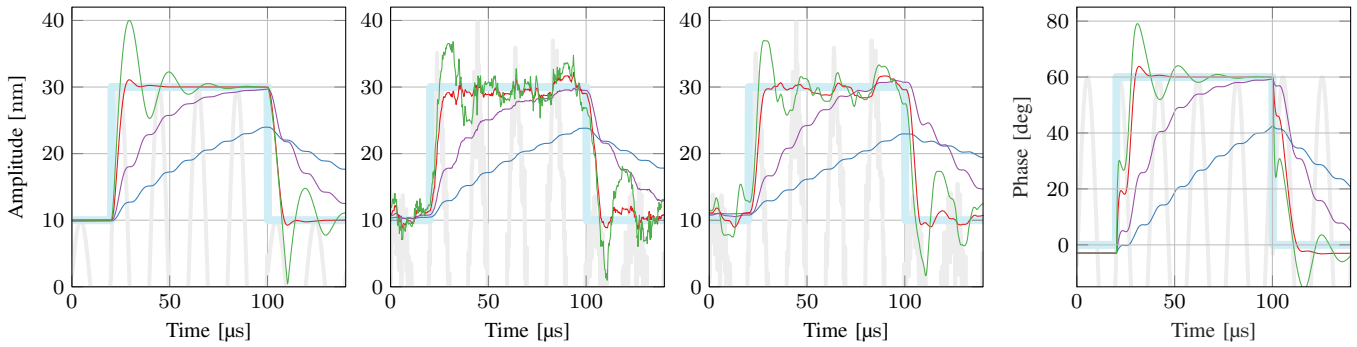

(a) Amplitude (b) Amplitude, Noise, $W = 1$ (c) Amplitude, Noise, $W = W_{LP}$ (d) Phase

Fig. 3. Step response simulation of the Lyapunov estimator for amplitude demodulation (a)-(c) and phase demodulation (d), with carrier frequency $f_0 = 50\,\text{kHz}$. Measurement noise with RMS $= 4\,\text{nm}$ added to (b)-(c) demonstrating difference in $W(s)$ filters, where $W_{LP}(s) = 1/(0.8\omega_0^{-1}s+1)$. Real amplitude/phase ( ), input signal ( ), demodulated amplitude $\widehat{a}$ or phase $\widehat{\phi}$ with $\gamma = 0.6f_0$ ( ), $\gamma = 2f_0$ ( ), $\gamma = 9f_0$ ( ), $\gamma = 24f_0$ ( ).

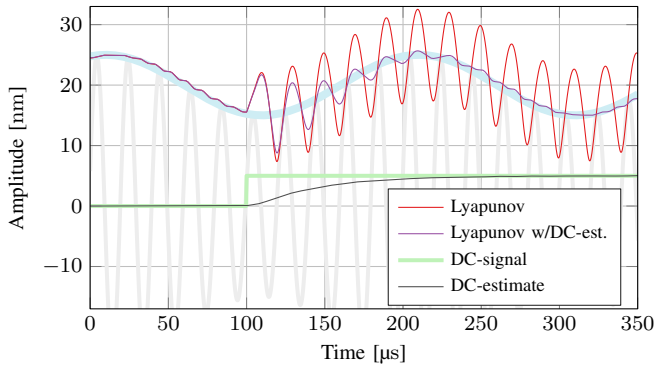

Fig. 4. Lyapunov estimator simulated with a step in DC-offset at the input signal, with carrier frequency $f_0 = 50\,\text{kHz}$, gain $\gamma = 9f_0$, and DC-gain $\gamma_{DC} = 20\,\text{k}$ for the augmented Lyapunov estimator with DC-estimation.

filter at the measured input signal. Another solution is to augment the Lyapunov estimator to simultaneously estimate the offset. This can be performed by adding a third state in $\widehat{\mathbf{x}}$ representing estimated offset, and adding a third constant element to $\mathbf{c}$ – typically 1. Finally, γ is modified to accept a different gain for the offset than for the amplitude/phase estimates, replacing it with the diagonal matrix

$$\mathbf{\Gamma} = \text{diag}(\gamma, \gamma, \gamma_{DC}) \tag{30}$$

where γ_{DC} is the DC-offset update gain, and (9) now assumes matrix multiplication. Since the offset is by definition slowly-varying, the DC-gain can be set relatively low to avoid affecting the performance of the demodulated signals. This implementation is demonstrated in Fig. 4 (purple line). It is seen that the oscillations in tracking response introduced with the DC-step is reduced once the DC-estimate converges. Conversely, the amplitude estimate of the original Lyapunov estimator continues with standing oscillations after the DC-offset is introduced.

VI. Experimental Results

A. Implementation Details

The Lyapunov estimator was implemented on a National Instruments USB-7855R with Kintex-7 70T FPGA using dedicated DSP blocks, achieving a sample frequency of 300 kHz. The performance of the implemented Lyapunov estimator was experimentally assessed and compared with a state-of-the-art lock-in amplifier (LIA, Zürich Instruments HF2LI) which provides flexible post-mixing low-pass filter (LPF) settings.

B. Amplitude Tracking Bandwidth

To determine the amplitude tracking bandwidth, a laboratory function generator (Agilent 33521A) is employed, providing a carrier frequency of 50 kHz amplitude modulated by a swept sine signal. This FM-AM concept directly reveals the LPF characteristic of the Lyapunov estimator and of the post-mixing filters of the LIA and allows for a direct extraction of the $-3\,\text{dB}$ tracking bandwidth.

The tracking bandwidth frequency responses of a slow LIA with LPF cut-off frequency $f_c = 500\,\text{Hz}$, fast LIA with $f_c = 50\,\text{kHz}$, slow Lyapunov estimator with $\gamma = 20\,\text{k}$ and fast Lyapunov estimator with $\gamma = 700\,\text{k}$ are shown in Fig. 5(a). The slow settings achieve a $-3\,\text{dB}$ bandwidth of around 500 Hz for both the LIA and Lyapunov estimator, while the fast settings achieve a $-3\,\text{dB}$ bandwidth of $48.2\,\text{kHz}$ and $50.0\,\text{kHz}$ for the LIA and Lyapunov estimator, respectively.

Note, that the fast LIA shows significant spikes at $2f_0$ and $4f_0$ due to insufficient filtering of the mixing products. To further highlight this point, time-domain tracking experiments of a square-modulated sine wave are shown in Fig. 5(b). Using the fast bandwidth setting for both demodulators, the LIA amplitude estimate is dominated by $2f_0$ oscillations, making this demodulator impractical at these tracking bandwidths.

The results emphasize the fact that the Lyapunov estimator is superior to the LIA when carrier frequencies are small compared to the necessary tracking bandwidth. While the tracking bandwidth of the LIA can be increased by choosing a large LPF cut-off frequency, the amplitude estimate becomes increasingly distorted by the mixing products.

The $-3\,\text{dB}$ tracking bandwidth of the Lyapunov estimator is plotted against the gain γ in Fig. 6, and compared to simulated values. The bandwidth increases approximately linearly with increasing γ until the bandwidth approaches the cantilever oscillation frequency f_0. There is a constant gain discrepancy between simulations and experiments, this can possibly be

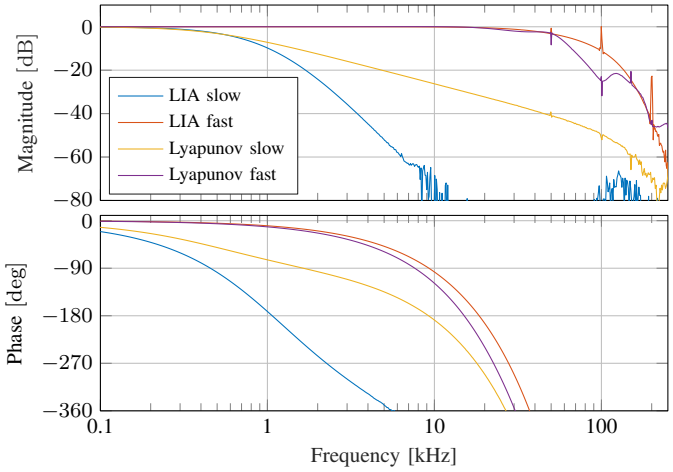

(a) Frequency response

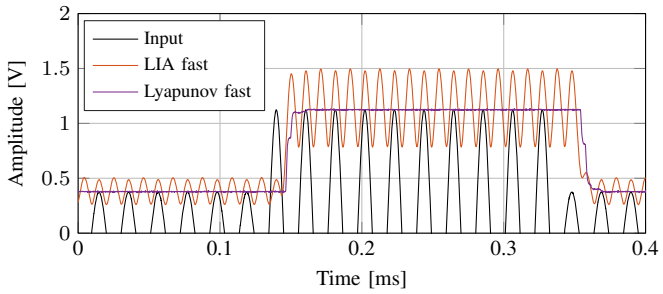

(b) Time-domain tracking

Fig. 5. Amplitude tracking experiment using the lock-in-amplifier and Lyapunov estimator with a carrier frequency of 50 kHz. (a) Frequency response at different bandwidth settings. (b) Time-domain tracking of a square-modulated sine wave.

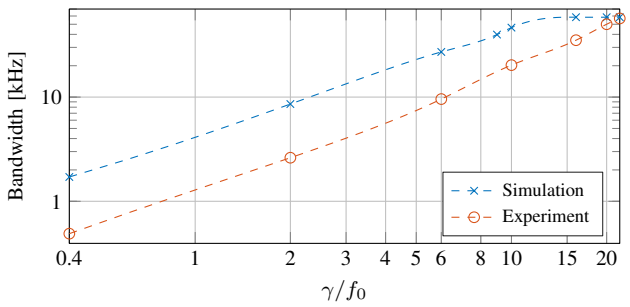

Fig. 6. Tracking response of Lyapunov estimator for increasing gain γ.

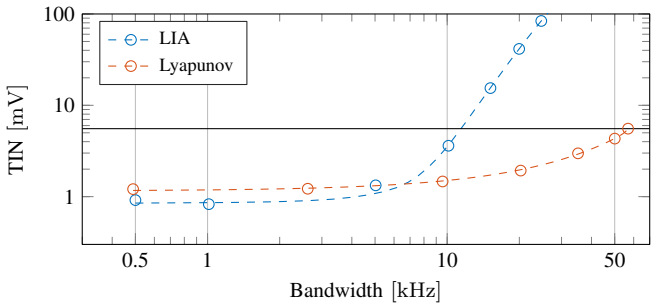

Fig. 7. Measured total integrated noise of amplitude estimate from LIA and Lyapunov estimator, with curve fit, as a function of tracking bandwidth.

attributed to internal gains in the experimental setup not accounted for.

C. Noise Analysis

In this experiment, the RMS noise of the amplitude estimate of the Lyapunov estimator and LIA is evaluated as a function of tracking bandwidth. For this purpose, the four channel acquisition front-end of a micro system analyzer (Polytec MSA-050-3D) is used to capture time-domain data passed through a high order anti-aliasing LPF with cut-off frequency of 1.2 MHz and sampled at $f_s = 2.56\,\mathrm{MHz}$ for $T = 13.11\,\mathrm{s}$. We use the total integrated noise (TIN) [21] as the performance metric which is obtained by integrating the noise density estimate from DC to $f_s/2$ using Welch's method [22] without averaging nor overlap.

The total integrated noise of the amplitude estimate obtained from the Lyapunov estimator is compared with the demodulated amplitude of the LIA as a function of the tracking bandwidth in Fig. 7. The RMS noise of the Lyapunov estimator estimate only increases slightly from $1.21\,\mathrm{mV}$ for the smallest bandwidth of $500\,\mathrm{Hz}$ to $5.6\,\mathrm{mV}$ for the largest bandwidth of $50\,\mathrm{kHz}$. In contrast, the RMS noise of the demodulated amplitude using a LIA, increases exponentially when the LPF cut-off frequency is increased above approximately $10\,\mathrm{kHz}$. While the LIA is better at very low bandwidths, above $7\,\mathrm{kHz}$ the Lyapunov estimator shows significantly lower noise. In other words, for the same TIN of $5.6\,\mathrm{mV}$, the LIA only achieves a $10\,\mathrm{kHz}$ bandwidth compared to almost $50\,\mathrm{kHz}$ achieved by the Lyapunov estimator. Thus, during high-speed experiments, the Lyapunov estimator could either track at the same bandwidth for a lower total integrated noise compared to the LIA – or at higher bandwidths for the same total integrated noise.

The improved LIA noise response at low bandwidths can be attributed to its higher order low-pass filtering. In fact, the Lyapunov estimator can be seen to act as a first-order LPF in the 1–10 kHz range based on its 20 dB/decade roll-off in Fig. 5(a), while the commercial LIA employs a fourth order Butterworth filter. As shown in the appendix, the TIN of the LIA is expected to be ~ 0.56 times the TIN of the Lyapunov estimator purely due to the different filter orders, while the experimental TIN ratio was measured to be 0.73. This may suggest that the Lyapunov estimator would outperform the LIA at the same filter order. However, other sources for the difference should be considered, including noise not being completely white, or measurement noise at higher frequencies not being filtered out. Additionally, the LIA has a fixed sampling rate about 3 orders of magnitude faster than the Lyapunov estimator, and the two estimators use different signal input ranges. This will in total result in some differences partly attributable to the experimental setup.

D. High-Speed AFM Imaging

Finally, the Lyapunov estimator and LIA is used in a high-speed constant-height tapping-mode AFM experiment for demonstrating the effect of increased demodulator bandwidth. The common z-axis actuator bandwidth limitation is circumvented by reducing the z-axis controller bandwidth to the point

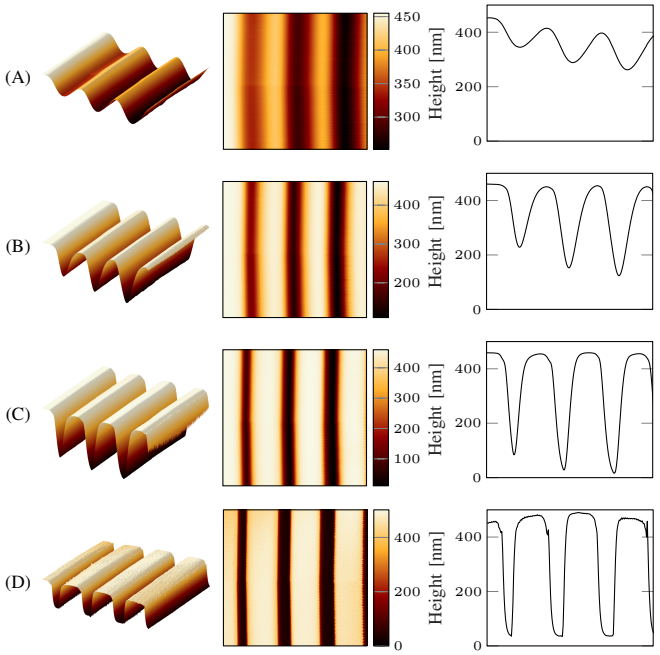

(a) 3D Image (b) 2D Image (c) Cross-section

Fig. 8. AFM scanning results. (A) LIA with $f_c = 100\,\text{Hz}$, (B) LIA with $f_c = 200\,\text{Hz}$, (C) LIA with $f_c = 400\,\text{Hz}$ and (D) Lyapunov estimator with $\gamma = 60 \times 10^3$, providing a tracking bandwidth of $\sim$1.6 kHz.

where the sample features during scanning entirely appear in the amplitude error image, thus reducing the bandwidth-limiting components of the AFM z-axis feedback loop to the cantilever and demodulator exclusively.

In order to render the demodulator the bottleneck of the open-loop AFM chain, a fast cantilever is necessary. Due to the sample frequency limitation of the labview FPGA, we employ a cantilever with fundamental resonance frequency of $f_0 \approx 50\,\text{kHz}$. The piezoelectric integrated actuation of the cantilever allows for model-based quality (Q) factor control to reduce the Q factor to $Q_0 = 8$ [23], resulting in an experimentally verified tracking bandwidth of $3.3\,\text{kHz}$ (not shown) which adequately matches the first order approximation $f_0/(2Q_0)$.

AFM images of a calibration grating (NT-MDT TGZ3) with periodic features of heights $h = 520 \pm 3\,\text{nm}$ were obtained on an NT-MDT NTEGRA AFM. The sample was scanned at a speed of $627.45\,\mu\text{m/s}$ in a $10 \times 10\,\mu\text{m}$ area at a scanner rate of $31.37\,\text{Hz}$ and resolution of 256×256 pixels, while recording the amplitude estimates of the LIA and the Lyapunov estimator in parallel. As only the forward trajectory is recorded, the entire image is acquired in 8.16 seconds.

The γ of the Lyapunov estimator could have been set according to (29) for the highest demodulator bandwidth. However, this initial value allows the Lyapunov estimator to track the amplitude at a much higher bandwidth than that of the cantilever tracking bandwidth. Instead, γ was reduced in order to improve the overall noise response of the system. The resulting gain was set to $\gamma = 1.2 f_0$ which results in a $-3\,\text{dB}$ bandwidth at approximately $1.6\,\text{kHz}$.

The high-speed constant height imaging results are presented in Fig. 8. Every experiment is performed at the same imaging speed, and each row represents increasing demodulator bandwidths. By setting a larger demodulator bandwidth, the sharp sample features are more accurately tracked as demonstrated by the consecutive rows, with the highest bandwidth here performed by the Lyapunov estimator in the last row.

VII. Conclusion

In this article, an amplitude and phase estimator designed for use in high-speed dynamic mode atomic force microscopy has been introduced. The Lyapunov estimator is designed for high-bandwidth, yet low complexity for ease of implementation. It requires no tuning by using the suggested gain for high-bandwidth performance in (29). However, the noise response can be improved by reducing the gain, such as by matching the resulting demodulator bandwidth to the bandwidth of the cantilever or z-axis actuator. It has also been demonstrated that the Kalman filter reduces to the Laypunov estimator under certain conditions. Experimental results, including AFM imaging with the estimator used for amplitude demodulation, demonstrates the high-bandwidth performance of the method.

Appendix
Total Integrated Noise

The total integrated noise (TIN) given white noise filtered through a system $G(s)$ is given by [21]

$$\sigma(G) = \sqrt{\int_0^{f_{bw}} A|G(j2\pi f)|^2 df} \tag{31}$$

where f_{bw} is the measurement bandwidth, and A is the power spectral density of the white noise. Consider the first order and second order low-pass filters

$$G_1(s) = \frac{1}{(2\pi f_c)^{-1}s + 1}, \quad G_2(s) = \frac{1}{((2\pi f_c)^{-1}s + 1)^2},$$

for some cut-off frequency $f_c > 0$. Using (31) the TIN for each system is given by

$$\sigma(G_1) = \sqrt{A}\sqrt{f_c \operatorname{atan}\left(\frac{f_{bw}}{f_c}\right)} \tag{32}$$

$$\sigma(G_2) = \sqrt{A}\sqrt{\frac{1}{2} f_c \operatorname{atan}\left(\frac{f_{bw}}{f_c}\right) + \frac{1}{2}\frac{f_{bw} f_c^2}{f_{bw}^2 + f_c^2}}. \tag{33}$$

It can be shown that $\sigma(G_1) > \sigma(G_2)$ for all $f_{bw}, f_c > 0$. Furthermore, consider the case where the measurement bandwidth is much greater than the cut-off frequency, $f_{bw} \gg f_c$. Then, the ratio between the TIN of each system is given by

$$\lim_{f_{bw}\to\infty} \frac{\sigma(G_2)}{\sigma(G_1)} = 1/\sqrt{2}.$$

Thus, the TIN of the second-order filter is a factor ~ 0.71 the TIN of the first-order low-pass filter. By following the above procedure for the higher order filters

$$G_n(s) = \frac{1}{((2\pi f_c)^{-1}s + 1)^n}, \tag{34}$$

the TIN ratio between an nth order and a first order low-pass filter can be found. Results are summarized in Table I. Note that the TIN is reduced with increasing filter order.

TABLE I

n	$\sigma(G_n)/\sigma(G_1)$
2	0.7071
3	0.6124
4	0.5590
5	0.5229

REFERENCES

[1] D. Y. Abramovitch, S. B. Andersson, L. Y. Pao, and G. Schitter, "A Tutorial on the Mechanisms, Dynamics, and Control of Atomic Force Microscopes," in *American Control Conference*, New York, USA, 2007, pp. 3488–3502.

[2] R. Garcia and R. Perez, "Dynamic atomic force microscopy methods," *Surface science reports*, vol. 47, no. 6-8, pp. 197–301, 2002.

[3] N. Jalili and K. Laxminarayana, "A review of atomic force microscopy imaging systems: application to molecular metrology and biological sciences," *Mechatronics*, vol. 14, no. 8, pp. 907–945, 2004.

[4] M. R. P. Ragazzon, M. Vagia, and J. T. Gravdahl, "Cell Mechanics Modeling and Identification by Atomic Force Microscopy," in *7th IFAC Symposium on Mechatronic Systems*, Loughborough, UK, 2016.

[5] T. Ando, T. Uchihashi, and T. Fukuma, "High-speed atomic force microscopy for nano-visualization of dynamic biomolecular processes," *Progress in Surface Science*, vol. 83, no. 7-9, pp. 337–437, 2008.

[6] Y. K. Yong, S. P. Wadikhaye, and A. J. Fleming, "High speed single- and dual-stage vertical positioners," *Review of Scientific Instruments*, vol. 87, no. 8, p. 085104, 2016.

[7] R. B. Northrop, *Introduction to instrumentation and measurements*, 2nd ed. Boca Raton, FL: CRC Press, 2005.

[8] T. Ando, N. Kodera, E. Takai, D. Maruyama, K. Saito, and A. Toda, "A high-speed atomic force microscope for studying biological macromolecules," *Proceedings of the National Academy of Sciences*, vol. 98, no. 22, pp. 12 468–12 472, 2001.

[9] D. Y. Abramovitch, "Low latency demodulation for Atomic Force Microscopes, Part I efficient real-time integration," in *American Control Conference*, 2011, pp. 2252–2257.

[10] K. S. Karvinen and S. O. R. Moheimani, "A high-bandwidth amplitude estimation technique for dynamic mode atomic force microscopy," *Review of Scientific Instruments*, vol. 85, no. 2, p. 023707, 2014.

[11] K. S. Karvinen, "Control and Estimation Techniques for High-Bandwidth Dynamic Mode Atomic Force Microscopy," Ph.D. dissertation, University of Newcastle, 2014.

[12] M. G. Ruppert, K. S. Karvinen, S. L. Wiggins, and S. O. R. Moheimani, "A Kalman Filter for Amplitude Estimation in High-Speed Dynamic Mode Atomic Force Microscopy," *Control Systems Technology, IEEE Transactions on*, vol. 24, no. 1, pp. 276–284, 2016.

[13] M. G. Ruppert, D. M. Harcombe, and S. O. R. Moheimani, "State Estimation for High-Speed Multifrequency Atomic Force Microscopy," in *American Control Conference*, Boston, USA, 2016.

[14] ——, "High-Bandwidth Demodulation in Multifrequency AFM: A Kalman Filtering Approach," *IEEE/ASME Transactions on Mechatronics*, vol. PP, no. 99, 2016.

[15] M. R. P. Ragazzon, J. T. Gravdahl, and A. J. Fleming, "On Amplitude Estimation for High-Speed Atomic Force Microscopy," in *American Control Conference*, Boston, USA, 2016.

[16] P. A. Ioannou and J. Sun, *Robust adaptive control*. Upper Saddle River, NJ: Prentice Hall, 1996.

[17] R. G. Lyons, *Understanding Digital Signal Processing*, 3rd ed. Upper Saddle River, NJ: Prentice Hall, 2010.

[18] O. Egeland and J. T. Gravdahl, *Modeling and Simulation for Automatic Control*. Trondheim, Norway: Marine Cybernetics, 2002.

[19] B. Brogliato, B. Maschke, R. Lozano, and O. Egeland, *Dissipative Systems Analysis and Control*. London, UK: Springer, 2007.

[20] K. S. Narendra and L. S. Valavani, "Stable Adaptive Controller Design–Direct Control," *IEEE Transactions on Automatic Control*, vol. 23, no. 4, pp. 570–583, 1978.

[21] A. J. Fleming and K. K. Leang, *Design, Modeling and Control of Nanopositioning Systems*. Cham, Switzerland: Springer, 2014.

[22] J. G. Proakis and D. G. Manolakis, *Digital signal processing: Principles, algorithms, and applications*, 3rd ed. Upper Saddle River, NJ: Prentice Hall, 1996.

[23] M. G. Ruppert and S. O. R. Moheimani, "Multimode Q Control in Tapping-Mode AFM: Enabling Imaging on Higher Flexural Eigenmodes," *IEEE Transactions on Control Systems Technology*, vol. 24, no. 4, pp. 1149–1159, 2016.